

# Micromechanical Strength of Individual Al<sub>2</sub>O<sub>3</sub> Platelets

Ezra Feilden<sup>a,\*</sup>, Tommaso Giovannini<sup>a,b</sup>, Na Ni<sup>a,\*</sup>, Claudio Ferraro<sup>a</sup>, Eduardo Saiz<sup>a</sup>, Luc Vandeperre<sup>a</sup>, Finn Giuliani<sup>a,b</sup>

<sup>a</sup> Centre of Advanced Structural Ceramics, Department of Materials, Imperial College London, SW7 2AZ, UK

<sup>b</sup> Department of Mechanical Engineering, Imperial College London, SW7 2AZ, UK

\* Corresponding Author; Ezra Feilden [ef509@ic.ac.uk](mailto:ef509@ic.ac.uk)

## Abstract

Optimising the properties of platelet reinforced composites requires the strength of the reinforcing phase to be known, however strength measurements at such small scales are difficult and therefore data is sparse. In this work the flexural strength and Weibull modulus of microscopic, alumina platelets has been measured as  $5.3 \pm 1.3$  GPa and 3.7 respectively, using an *in-situ* micro 3-point bend test. A general approach to correct for the effect of variation in sample size on the Weibull modulus is presented, and the internal structure of the platelets is revealed by TEM.

Keywords: Ceramic, Flexural Strength, 3 Point Bending, In-situ, Sapphire

## Main Text

The advance of many modern technologies requires the use of materials that can simultaneously be lightweight, strong and tough. Often these properties are mutually exclusive in bulk materials, and so diverse composite systems are needed, taking advantage of the constituent properties of each component. This design principle has led to the development of long fibre reinforced composites, which have been particularly successful and find mature applications in many fields. While exhibiting some remarkable mechanical properties, these materials are notoriously difficult and expensive to produce, mostly due to the processing requirements of the long fibres.[1] For this reason other composite systems have been explored, such as short fibres, platelets and particle composites.[2] The introduction of these smaller reinforcing phases within a matrix allows for simpler production processes, however they have some drawbacks, such as inhalation risks or lower reinforcing capacities compared with long fibres. A large number of recent studies have demonstrated the potential of platelet-like reinforcements, specifically micron-scale Al<sub>2</sub>O<sub>3</sub> platelets. These particular platelets have been used extensively in other composite studies.[3–8] These platelets are favoured as they are oxidation resistant, stable, crystalline and can be mass produced with a consistent morphology. Despite the interest they have received, the mechanical properties of individual platelets are still unknown. These properties are needed when designing composites as they allow for the interfacial strength to be tailored to maximise the reinforcing and toughening effect of the platelets, and thus optimise the mechanical properties of the material.

The aim of this work was therefore to determine the mechanical performance of single platelets by performing *in-situ* micro-bending tests. To achieve this goal ~0.01g of alumina platelets (obtained in bulk from Advanced Nano Technologies Ltd) were scattered on a silicon wafer. Individual platelets were then welded to a tungsten OmniProbe 200 micromanipulator and

1 elevated away from the substrate. The platelets were milled into regular rectangles using a  
2 focused ion beam. All sample preparation was performed using a Helios NanoLab FIB/SEM  
3 equipped with a Pt gas injection system for welding and a Ga source for milling. Each platelet  
4 was then placed across pre-milled trenches, welded at one edge of the trench, and the probe tip  
5 removed by FIB milling, as shown in Figure 1a-f. All milling was carried out with a current  
6 below 0.92 nA and all welding with a current below 0.28 nA. Although it is performed on a  
7 smaller length scale, this technique bears some resemblance to previous work[9–11].  
8 Mechanical testing of the samples was performed by using a nano-indentation rig (Alemnis  
9 GmbH, CH) developed for *in-situ* testing inside an SEM. The load was applied by means of a 60°  
10 diamond wedge with a radius of 100 nm. To allow for alignment of the tip perpendicular to the  
11 beam length, samples were mounted on top of a rotational stage. All specimens were loaded in  
12 displacement control using a displacement rate of 5 nm s<sup>-1</sup> to the point of failure. To gain further  
13 insight on the defects causing failure, selected platelets were prepared for observation under  
14 TEM by FIB milling (2–30 keV Ga<sup>+</sup> incident beam energy with currents of 16 pA – 21 nA). TEM  
15 and energy-dispersive x-ray spectroscopy (EDX) was carried out on a FEI Titan 80-300 S/TEM  
16 at 300 kV equipped with a windowless EDX detector (Bruker QUANTAX 400-STEM). Focal series  
17 micrographs were acquired using a spherical aberration coefficient Cs ~ -2 μm and exit-wave  
18 reconstruction was performed using TruImage software (FEI).  
19  
20  
21

22 The results from this procedure are presented in Table 1 and Figure 2. The macroscopic  
23 bending strength of single crystal alumina typically ranges from 0.5-1.0 GPa,[12,13] which is  
24 substantially lower than the average bending strength of 5.3 GPa observed here, while  
25 microscopic sapphire fibres have been shown to possess strength of 2.9 GPa.[14] This is in  
26 accordance with previous studies where large increases in strength at small scales have been  
27 extensively reported for a range of materials.[10,15] This result can be correlated with the  
28 lower probability of finding defects within smaller sized samples, and with the smaller size of  
29 these critical defects. In our case a spherical defect cannot be larger than 0.9-0.4 μm (the range  
30 of platelet thicknesses tested). However if we scale the characteristic strength of the platelets to  
31 typical macroscopic dimensions (2.5x2.5x25mm)[12] then the expected strength would be just  
32 0.01-0.1 GPa, therefore in proportion to macroscopic sapphire the platelets are significantly  
33 more defective.  
34  
35  
36  
37

38 The force-displacement curves show a linear trend, however a small drop was often observed at  
39 low loads, as shown in Figure 2a. This point corresponds to the platelet detaching from the  
40 substrate where it is being held either by a small Pt weld or by surface forces. By the time of  
41 failure all platelets had detached from the substrate and were bending freely. At these scales  
42 plastic deformation is a possibility, but it is unlikely that these platelets are experiencing a high  
43 enough shear stress, 4.3-10.7 GPa,[16] to allow slip to occur. Also, all loading curves were  
44 observed to be linear until failure.  
45  
46

47 Due to the small data set size, the Weibull modulus,  $m$ , of the platelets was calculated using the  
48 probability estimator  $P_f = \frac{i-0.3}{N+0.4}$ [17] where  $i$  is the rank of the platelet strength and  $N$  is the set  
49 size (10 samples), which was then used to construct a Weibull plot. From this plot the  
50 characteristic stress,  $\sigma_0$ , was found to be 5.82 GPa. Typical Weibull analysis assumes all of the  
51 tested samples to be of identical dimensions, however this is not practical in this test due to  
52 variation in the thickness and morphology of the platelets. Therefore, a more complete analysis,  
53 derived elsewhere[18] and given in the supplementary information, was developed to offset the  
54 effect of variation in sample area and volume on  $m$ . The procedure consists of correcting the  
55 effective failure strength for sample area or volume using equations 1 or 2:  
56  
57  
58  
59  
60  
61  
62  
63  
64  
65

$$\sigma_{i \text{ area corrected}} = \left( \frac{l_i w_i}{A_{\text{ref}}(m+1)} \right)^{1/m} \cdot \sigma_i \quad (1)$$

$$\sigma_{i \text{ volume corrected}} = \left( \frac{l_i w_i t_i}{2V_{\text{ref}}(m+1)^2} \right)^{1/m} \cdot \sigma_i \quad (2)$$

(where  $l$  is the bar length,  $w$  is the bar width,  $t$  is the bar thickness,  $m$  is the Weibull modulus,  $A_{\text{ref}}$  is the reference area,  $V_{\text{ref}}$  is the reference volume), and calculating the Weibull modulus using the corrected stress values. As the expression for the corrected stress involves  $m$ , it can only be solved iteratively by first assuming  $m$  from the uncorrected data then cyclically calculating the new  $m$  until its value converges. Convergence typically occurs to two decimal places after 3-4 iterations. This adjustment accounts for differences in volume or area between the samples in the 3 point bending configuration, allowing for the strength of a reference size to be estimated for each sample. This method may prove to be a useful general tool in other applications requiring Weibull analysis of non-uniform samples in 3 point bending.

Either the area correction or the volume correction should be used depending on whether the critical defects are expected to exist on the surface of the samples, or within the samples. When corrected for area, the Weibull modulus decreases from 3.9 to 3.7, and for volume it increases from 3.9 to 4.0. These moduli are similar in magnitude to other brittle materials tested in this configuration,[9,14] especially if the uncertainty on the Weibull modulus estimate from small sample sizes is considered.[19] The different crystallographic orientations of the platelets may contribute to the scatter in measured strengths, as the fracture energy of alumina can vary by a factor of 2.3 between different fracture planes[20]. The distribution of defects in the platelets, and measurement uncertainties in the procedure may also contribute to the data scatter, and therefore lower the Weibull modulus. These effects are thought to be minimal for macroscopic tests,[21] however we have found that measurement uncertainties can give rise to >10% variation in measured strength, therefore this might significantly lower the apparent Weibull modulus.

While we have not measured the toughness,  $K_{1c}$ , of the platelets, it is most likely within the range between the value calculated from the surface energy (2.12 MPa $\sqrt{\text{m}}$ )[22] to the value measured from macroscopic tests of sapphire (2.35 MPa $\sqrt{\text{m}}$ )[23]. Assuming a shape factor of 1.36,[24] the average defect size was calculated to be 28-34 nm. Two possible candidates for the critical defects are surface defects, and growth defects inside the sample. Step edges have been observed on platelet surfaces, as shown in Figure 2g-h, which could act as stress concentrators when oriented correctly. SEM measurements of side-on platelets revealed these steps to be ~10-30 nm in height, so they are in the correct size range to be responsible for failure. TEM analysis of one platelet revealed a complex defective region in the centre of the platelets roughly 50nm thick, flanked by perfect crystalline  $\alpha\text{-Al}_2\text{O}_3$  on either side, oriented with the [0001] direction perpendicular to the platelet surface. High-resolution TEM (Figure 2d-e) and electron diffraction (supplementary information) of this central region suggests the presence of stacking faults and impurities that were identified by EDS to be sodium and fluorine, as shown in Figure 3. Dislocations and nano-twinning were also identified, see supplementary information. Impurities remaining from the growth process have been observed at the central twin plate of topotaxially grown alumina platelets in other work,[25] it is therefore likely that these platelets also possess this feature in the form of Na and F. Upon bending, the region of the specimen which experiences the highest tensile stress is the bottom face of the bar. Considering these defects lie close to the neutral axis of the bar, where tensile stress is at a minimum, they cannot be responsible for the mode-I failure of the samples. Most platelets were ejected from the test area and lost when they failed, however some remained on the trench allowing for analysis of

1 the fracture surface. In some cases, the crack was observed to propagate in mode-I to the middle  
2 of the platelet, then deflect into mode-II parallel to the surface, thus we propose that these  
3 platelets typically fail by mode-I fracture starting at step edges and other surface defects, and  
4 the crack is then occasionally deflected by the defective central region and turns into mode-II  
5 (see Figure 2f). As we expect the surface defects to be responsible for failure, then we can take  
6 the area-adjusted Weibull modulus, 3.7, as the true Weibull modulus. Previous work has  
7 suggested that the minimum criteria for a crack to deflect at an interface is that the fracture  
8 energy of the interfacial material is less than a quarter of the bulk fracture energy,[26] therefore  
9 the middle defective region must possess a less than a quarter of the fracture energy than that  
10 of the rest of the platelet.  
11

12 In summary, the flexural strength and Weibull modulus of topotaxially grown alumina platelets  
13 have been measured to be 5.3 GPa and 3.7 respectively. The average defect size was calculated  
14 to be 28-34 nm, and through analysis of the platelet surfaces as well as the interior of the  
15 platelets we were able to suggest some candidates for the critical defects in this material. These  
16 basic data can help the design process and selection of interfacial strengths in composites which  
17 use these platelets, allowing their mechanical properties to be fully optimised.  
18  
19  
20

## 21 Acknowledgments

22 The authors would like to thank the CASC industrial consortium and the Engineering and  
23 Physical Sciences Research Council (EPSRC) for the funding of this work. NN would like to  
24 acknowledge the funding from Imperial College Research Fellowship. We would also like to  
25 thank Advanced Nano Technologies Ltd. for providing the alumina platelets.  
26  
27  
28

## 29 References

- 30 [1] S.J. Park, B.J. Kim, Carbon Fibers and Their Composites, CRC Press, 2005.  
31 [2] H. Zhang, Z. Zhang, C. Breidt, Compos. Sci. Technol. 64 (2004) 2021–2029.  
32 [3] H. Le Ferrand, F. Bouville, T.P. Niebel, A.R. Studart, Nat. Mater. 14 (2015).  
33 [4] F. Bouville, E. Maire, S. Meille, B. Van de Moortèle, A.J. Stevenson, S. Deville, Nat. Mater. 13 (2014) 508–514.  
34 [5] D.K. Shukla, S. V. Kasisomayajula, V. Parameswaran, Compos. Sci. Technol. 68 (2008) 3055–3063.  
35 [6] L.J. Bonderer, A. Studart, L.J. Gauckler, Science (80-. ). 319 (2008) 1069–1073.  
36 [7] R.M. Erb, R. Libanori, N. Rothfuchs, A. Studart, Science (80-. ). 335 (2012) 199–204.  
37 [8] M. Kotoul, J. Pokluda, P. Šandera, I. Dlouhý, Z. Chlup, A.R. Boccaccini, Acta Mater. 56 (2008) 2908–2918.  
38 [9] M.G. Mueller, M. Fornabaio, G. Žagar, A. Mortensen, Acta Mater. 105 (2016) 165–175.  
39 [10] G. Žagar, V. Pejchal, M.G. Mueller, A. Rossoll, M. Cantoni, A. Mortensen, Acta Mater. 100 (2015) 215–223.  
40 [11] C. Ferraro, E. García-Tuñón, V. G. Rocha, S. Barg, M.D. Fariñas, T.E.G. Álvarez-Arenas, G. Sernicola, F. Giuliani,  
41 E. Sáiz, Adv. Mater. (2016) 12.  
42 [12] P. Gurjyants, M. Starostin, V.N. Kurlov, F. Théodore, J. Delepine, J. Cryst. Growth 198–199 (1999) 227–231.  
43 [13] C.A. Klein, J. Appl. Phys. 96 (2004) 3172–3179.  
44 [14] J.B. Davis, J. Yang, A.G. Evans, Acta Metall. Mater. 43 (1995) 259–268.  
45 [15] N. Jaya, M. Alam, Curr. Sci. 105 (2013) 1073–1099.  
46 [16] A. Montagne, S. Pathak, X. Maeder, J. Michler, Ceram. Int. 40 (2014) 2083–2090.  
47 [17] B. Bergman, J. Mater. Sci. Lett. 3 (1984) 689–692.  
48 [18] R. Danzer, T. Lube, P. Supancic, R. Damani, Ceramics Science and Technology- Set, Chapter 12- Fracture of  
49 Ceramics, 548-555, 2013.  
50  
51  
52  
53  
54  
55  
56  
57  
58  
59  
60  
61  
62  
63  
64  
65

- [19] J.E. Ritter, in: *Fract. Mech. Ceram.*, Plenum Press, 1983, pp. 227–249.
- [20] P. Becher, *J. Am. Ceram. Soc.* 59 (1976) 59–61.
- [21] R. Bermejo, P. Supancic, R. Danzer, *J. Eur. Ceram. Soc.* 32 (2012) 251–255.
- [22] S.M. Wiederhorn, *Annu. Rev. Mater. Sci.* 14 (1984) 373–403.
- [23] M. Yoshinori, Y. Wang, *J. Biomed. Mater. Res. - Part A* 28 (1994) 813–817.
- [24] N. Alford, J. Birchall, K. Kendall, *Nature* 330 (1987) 51–53.
- [25] E.A.D. White, J.D.C. Wood, *J. Mater. Sci.* 9 (1974) 1999–2006.
- [26] M.Y. He, A.G. Evans, *Int. J. Solids Struct.* 31 (1994) 3443–3455.

1  
2  
3  
4  
5  
6  
7  
8  
9  
10  
11  
12  
13  
14  
15  
16  
17  
18  
19  
20  
21  
22  
23  
24  
25  
26  
27  
28  
29  
30  
31  
32  
33  
34  
35  
36  
37  
38  
39  
40  
41  
42  
43  
44  
45  
46  
47  
48  
49  
50  
51  
52  
53  
54  
55  
56  
57  
58  
59  
60  
61  
62  
63  
64  
65

Table 1- Dimensions and calculated strengths of the platelets tested.

ID	l ( $\mu\text{m}$ )	h ( $\mu\text{m}$ )	w ( $\mu\text{m}$ )	f <sub>max</sub> (mN)	Strength (GPa)
1	5.30	0.41	2.58	0.34	6.1
2	5.65	0.60	2.12	0.65	7.2
3	5.65	0.87	2.76	1.14	4.7
4	5.57	0.94	3.18	1.07	3.2
5	5.57	0.43	2.78	0.39	6.4
6	5.57	0.51	2.15	0.24	3.6
7	5.57	0.44	5.02	0.67	5.8
8	5.57	0.51	3.82	0.63	5.3
9	5.57	0.50	3.30	0.38	3.9
10	5.57	0.79	3.35	1.61	6.5
				Average	5.3
				Std. Dev.	1.3

Figure 1  
[Click here to download high resolution image](#)

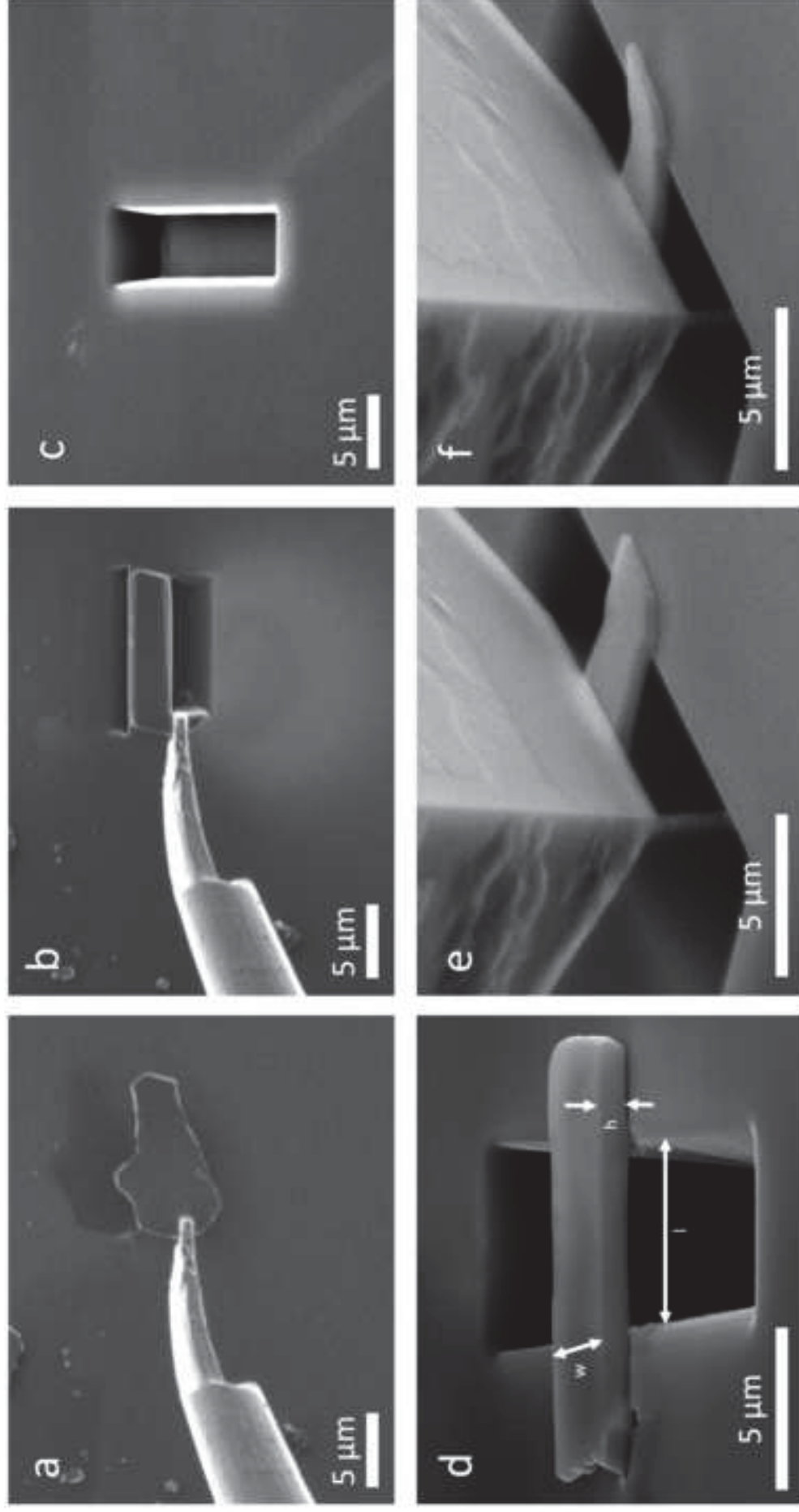


Figure 2  
[Click here to download high resolution image](#)

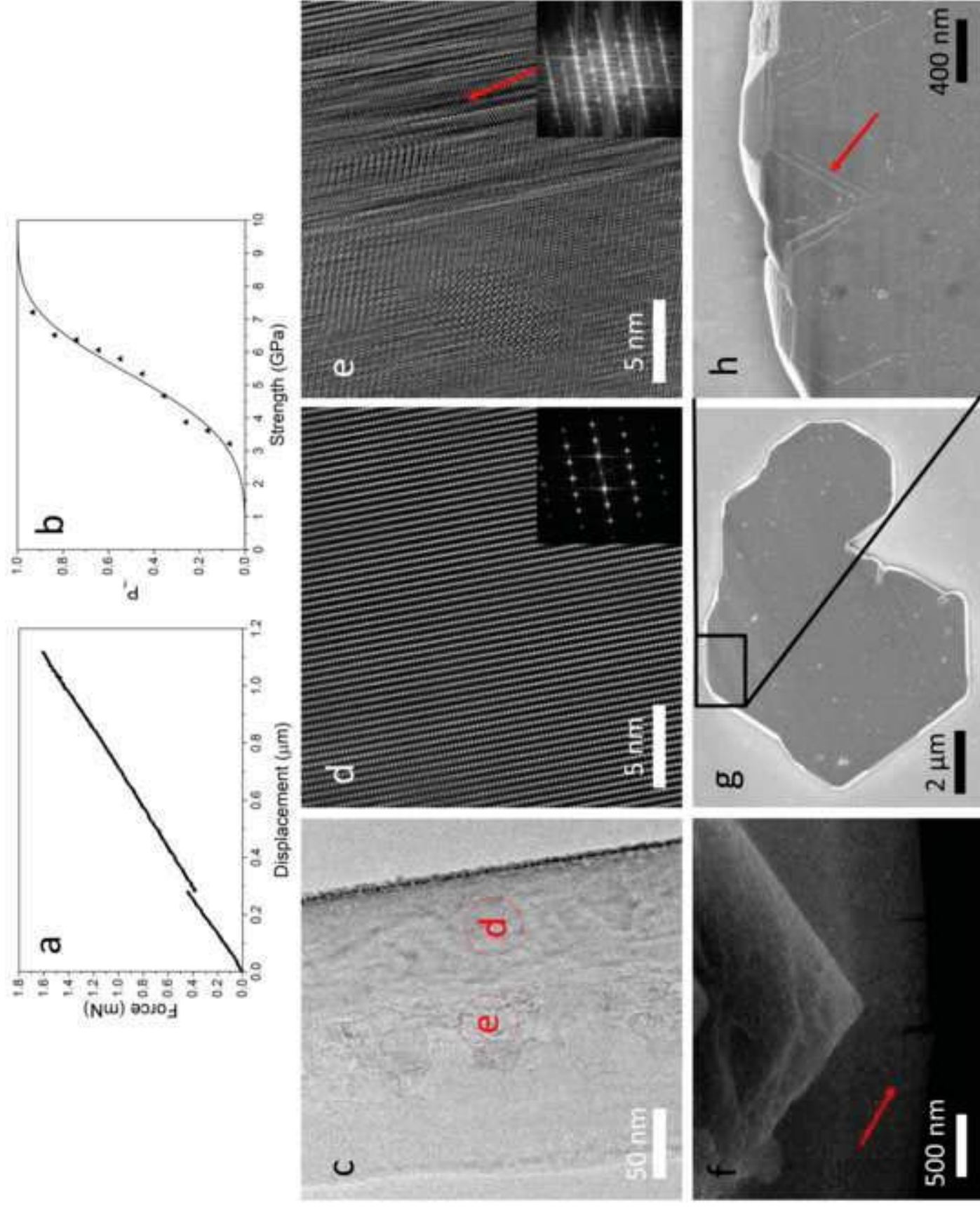




Figure 3  
[Click here to download high resolution image](#)

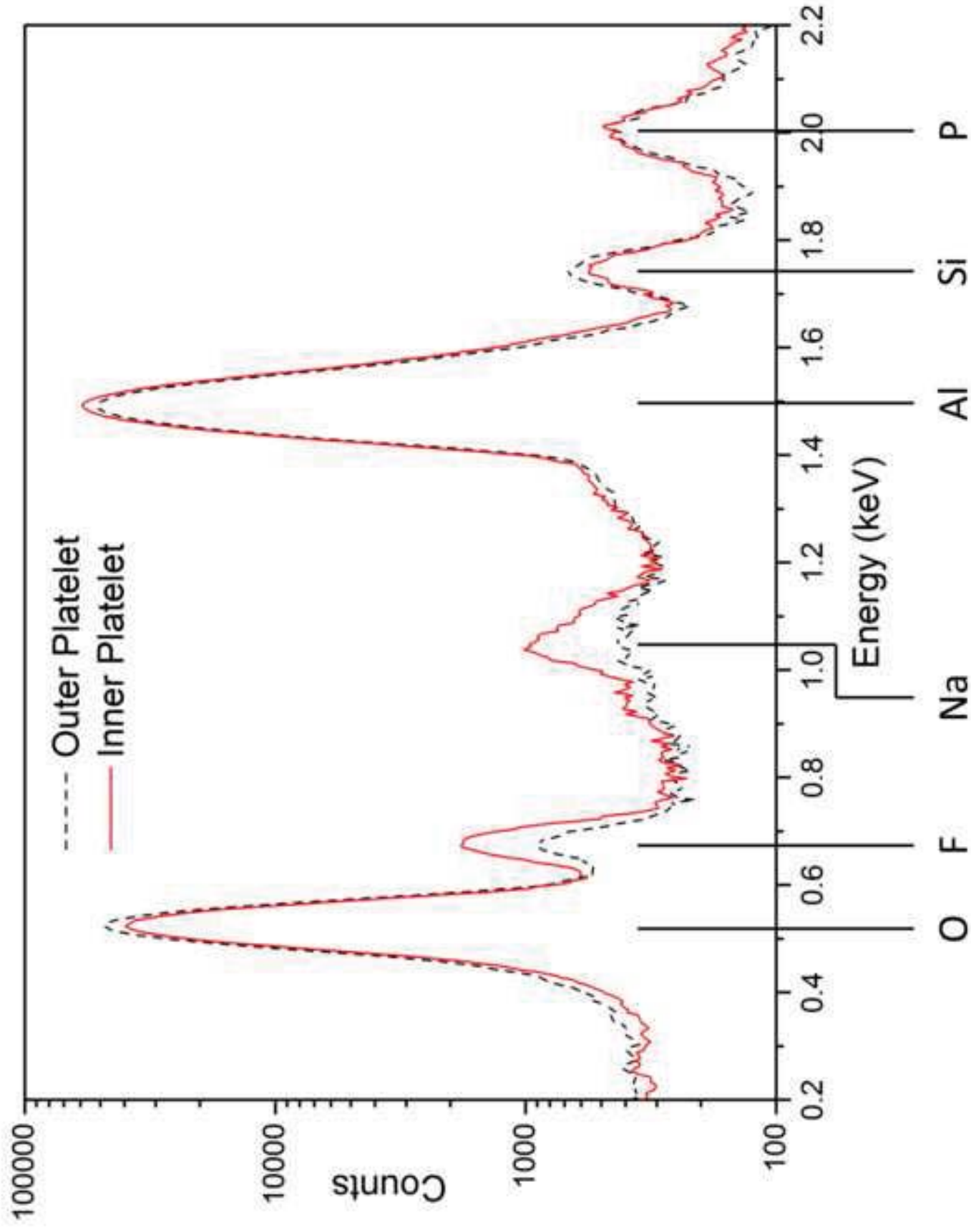


Figure 1- a- SEM image showing the pickup of a platelet by welding to a probe with Pt. b- FIB milling of the platelet into a bar shape while suspended above the substrate. c- Milling of a trench. d- Placement of the platelet ready for testing and the specification of the platelet dimensions used throughout. e,f- Contact and testing of a platelet with the diamond wedge.

Figure 2- a- Example force/displacement curve until failure for a test where the platelet detached from the substrate at  $\sim 0.4\text{mN}$ . b- Distribution of bending strength plotted against estimated probability of failure for the raw data, with the continuous Weibull distribution from the found parameters plotted. c- TEM bright field image showing the cross section of a platelet. The regions on the left and right are defect free, while the region in the centre is highly disordered. d,e- High resolution TEM images of the regions marked in c, alongside their fast Fourier transform (FFT) patterns. f- SEM image of a beam during testing, with deflection to mode-II crack propagation down the centre of a platelet indicated. g,h- Indicated growth steps on the surface of a representative platelet.

Figure 3- EDS Spectra gathered from the central defective region of a platelet and from a defect-free region of a platelet. F and Na were detected in much greater concentration in the central region, indicating the presence of impurities.

**Supplementary Material**

[Click here to download Supplementary Material: Sup Info new.docx](#)

**Supplementary Video**

[Click here to download Supplementary Material: F3s.mp4](#)